IOPscience iopscience.iop.org

Home Search Collections Journals About Contact us My IOPscience

Mean-field theory of charge ordering and phase transitions in the colossal-magnetoresistive manganites

This article has been downloaded from IOPscience. Please scroll down to see the full text article.

1999 J. Phys.: Condens. Matter 11 8561

(http://iopscience.iop.org/0953-8984/11/43/320)

View the table of contents for this issue, or go to the journal homepage for more

Download details:
IP Address: 128.206.162.204
The article was downloaded on 22/12/2010 at 19:03

Please note that terms and conditions apply.

J. Phys.: Condens. Matter **11** (1999) 8561–8578. Printed in the UK PII: S0953-8984(99)03919-3

Mean-field theory of charge ordering and phase transitions in the colossal-magnetoresistive manganites

S K Mishra†§, Rahul Pandit‡‖ and S Satpathy†

† Department of Physics and Astronomy, University of Missouri, Columbia, MO 65211, USA

‡ Centre for Condensed Matter Theory, Department of Physics, Indian Institute of Science, Bangalore-560 012, India

Received 4 May 1999, in final form 23 August 1999

Abstract. We study phase transitions in the colossal-magnetoresistive manganites by using a mean-field theory both at zero and non-zero temperatures. Our Hamiltonian includes double-exchange, superexchange, and Hubbard terms with on-site and nearest-neighbour Coulomb interaction, with the parameters estimated from earlier density-functional calculations. The phase diagrams show magnetic and charge-ordered (or charge-disordered) phases as a result of the competition between the double-exchange, superexchange, and Hubbard terms, the relative effects of which are sensitively dependent on parameters such as doping, bandwidth, and temperature. In accord with the experimental observations, several important features are reproduced from our model, namely, (i) a phase transition from an insulating, charge-ordered antiferromagnetic to a metallic, charge-disordered ferromagnetic state near dopant concentration $x = 1/2$, (ii) the reduction of the transition temperature $T_{AF\rightarrow F}$ by the application of a magnetic field, (iii) melting of the charge order by a magnetic field, and (iv) phase coexistence for certain values of temperature and doping. An important feature, not reproduced in our model, is the antiferromagnetism in the electron-doped systems, e.g., $La_{1-x}Ca_xMnO_3$ over the entire range of $0.5 \leqslant x \leqslant 1$, and we suggest that a multi-band model which includes the unoccupied t_{2g} orbitals might be an important ingredient for describing this feature.

1. Introduction

There have been many studies of doped manganites of the form $Ln_{1-x}A_xMnO_3$, where Ln is a rare earth like La, Nd, Pr and A is a divalent cation like Ca, Sr, Ba, Pb. Work in the 1950s and 1960s elucidated the nature of the magnetic ordering in these systems [1–3] and uncovered the role of the double-exchange mechanism in stabilizing ferromagnetic phases [4–6]. Recent work, motivated by the observation [7–12] of colossal magnetoresistance (CMR) in this class of compounds, has focused on their intriguing magnetic and conduction properties. We refer the reader to recent reviews [13, 14] for a survey of such studies.

For our purposes here, it suffices to note the following features of these doped manganites. The parent compounds are antiferromagnetic insulators; e.g., $LaMnO_3$ has an alternating antiferromagnetic arrangement of ferromagnetically ordered planes. When $LaMnO_3$ is doped, ferromagnetic phases are stabilized via the double-exchange mechanism as in $La_{1-x}Ca_xMnO_3$, which is a ferromagnetic metal for $0.1 \lesssim x \lesssim 0.5$. Further doping yields phases, often

§ Present address: Department of Materials Science and Engineering, Massachusetts Institute of Technology, Cambridge, MA-02139, USA.

‖ Also at: Jawaharlal Nehru Centre for Advanced Scientific Research, Bangalore, India.

0953-8984/99/438561+18$30.00 © 1999 IOP Publishing Ltd

with complex structures, that are antiferromagnetic insulators [15, 16]. In addition, these magnetically ordered phases can be charge ordered or charge disordered; for $x = 0.5$ this can be thought of as Mn^{3+} ions on one sublattice and Mn^{4+} ions on the other, though fluctuations often reduce such complete charge disproportionation. In some cases, as the temperature T is increased, insulator–metal transitions are seen; these are driven by the destruction of charge ordering, reminiscent of the Verwey transition in magnetite [17], but, unlike the case for magnetite, with an accompanying antiferromagnet-to-ferromagnet transition. For instance, at low T, $Nd_{0.5}Sr_{0.5}MnO_3$ is a charge-ordered antiferromagnet that has the complex CE structure [3] and undergoes a first-order transition to a charge-disordered ferromagnet when T is raised [2, 12, 18, 19].

Doping-driven, first-order ferromagnet-to-antiferromagnet transitions (presumably associated with charge ordering) have also been reported for $La_{1-x}Ca_xMnO_3$ [15, 16], though the question of first-order phase coexistence has not been investigated sufficiently, as we discuss later. The transition from a charge-ordered antiferromagnetic insulator (AFO) to a charge-disordered (or charge-non-ordered) ferromagnetic metal (FN) can also be obtained by changing the magnetic field H; e.g., in both $Pr_{0.5}Sr_{0.5}MnO_3$ and $Nd_{0.5}Sr_{0.5}MnO_3$ [18, 20] the transition temperature $T_{AF\rightarrow F}$ decreases rapidly with increasing H. There is also growing evidence that charge ordering in $Ln_{1-x}A_xMnO_3$ is related to the width of the e_g band, which is in turn determined by the average radius $\langle r_A\rangle$ of the A-site cations [13]: if $\langle r_A\rangle \lesssim 1.18$, only charge ordering is observed; if $1.18 \lesssim \langle r_A\rangle \lesssim 1.25$, charge ordering is observed at low T but a metallic ferromagnet (FN) appears as T is raised; if $1.25 \lesssim \langle r_A\rangle$, only an FN phase is observed.

The broad aim of our present study is to understand the phenomena of charge ordering, phase coexistence, and metal–insulator and magnetic phase transitions on the basis of a minimal model. Notice that we do not discuss orbital ordering in our model. To describe orbital ordering properly, phonon degrees of freedom—specifically, the coupling of the Jahn–Teller distortions of the MnO_6 octahedra to the electronic states—has to be included. This can be done without much difficulty, but it makes the numerical calculations much more involved and complicates the issues that we discuss in this paper. Instead, we take the point of view that, if charge ordering exists, then an orbital ordering may follow, driven by the local Jahn–Teller distortions of the MnO_6 octahedra. In some sense, this point of view is similar to the description of charge ordering in magnetite within the one-band Cullen–Callen model [22, 23] for the Verwey transition. We show that the coupled magnetic and charge-order transition observed in these materials, specifically at or near $x = 1/2$, is described very well by an electronic Hamiltonian which, in addition to the double-exchange term, includes the Hubbard and extended-Hubbard (nearest-neighbour) Coulomb interactions. As already mentioned, our model does not contain an explicit electron–phonon coupling, although the static Jahn–Teller distortion in $LaMnO_3$ is used to argue for the simple one-band model that we use. We believe that, as far as charge ordering is concerned, electron–electron interactions are the *principal* driving mechanism; electron–phonon interactions, beyond those responsible for the static Jahn–Teller distortion used implicitly in our model, merely renormalize electronic parameters.

The basic features of the electronic structure [24–26] of the CMR manganites are summarized as follows:

(1) The crucial states for the electron bands near the Fermi energy E_f consist of Mn_{3d} states with a small admixture of O_{2p} states; other levels, e.g., the La states, lie away from E_f.

(2) A large atomic exchange splitting ($\simeq$3 eV) raises the energy of the minority 3d spins on a given atom.

(3) Thus in $LaMnO_3$ the configuration of the Mn atom is $t_{2g}(3)e_g(1)$ whereas in $CaMnO_3$ it is $t_{2g}(3)$, with the Ca dopant in $La_{1-x}Ca_xMnO_3$ introducing holes into the system.

(4) The octahedral crystal field raises the energy of the e_g states with respect to the t_{2g} states by $\simeq$2 eV.
(5) A partially filled e_g band often leads to a Jahn–Teller distortion: for example, in $LaMnO_3$ the half-filling of the doubly degenerate e_g band leads to a Jahn–Teller distortion, which splits the e_g band into a lower $e_g(1)$ band and an upper $e_g(2)$ band, so band theory predicts correctly that $LaMnO_3$ is an insulator [24].
(6) In the double-exchange mechanism, the t_{2g} states are considered to form a localized spin $S = 3/2$, whereas the e_g states are considered delocalized; however, they interact with the localized spins via a Hund's-rule coupling J_H. This leads to an effective ferromagnetic coupling between the localized Mn spins in addition to the antiferromagnetic superexchange coupling J. If the e_g bands are either completely full or completely empty, the absence of conduction electrons suppresses the double-exchange mechanism.

The model Hamiltonian [27] that describes this physics is written as

$$\mathcal{H} = -t \sum_{\langle ij\rangle,\sigma} c^{\dagger}_{i\sigma} c_{j\sigma} + \text{h.c.} + U_0 \sum_i \hat{n}_{i\uparrow}\hat{n}_{i\downarrow} + U_1 \sum_{\langle ij\rangle,\sigma\nu} \hat{n}_{i\sigma}\hat{n}_{j\nu} - \tilde{J} \sum_{\langle ij\rangle} \boldsymbol{S}_i \cdot \boldsymbol{S}_j - 2\tilde{J}_H \sum_i \boldsymbol{S}_i \cdot \boldsymbol{s}_i - \mu \sum_{i\sigma} \hat{n}_{i\sigma} - \tilde{\boldsymbol{H}} \cdot \sum_i (\boldsymbol{S}_i + \boldsymbol{s}_i) \tag{1}$$

where the Hamiltonian is restricted to Mn sites on a simple-cubic lattice. Here t is the hopping amplitude for nearest-neighbour pairs of sites $\langle ij\rangle$, $c^{\dagger}_{i\sigma}$ and $c_{i\sigma}$ are, respectively, creation and annihilation operators for electrons on site i with spin σ ($\sigma = \uparrow$ or $\downarrow$), $\hat{n}_{i\sigma}$ is the associated number operator, μ is the chemical potential which controls the mean filling if we work in the grand-canonical ensemble, $\tilde{\boldsymbol{H}}$ is the external magnetic field, which couples both to the localized Mn spin $\boldsymbol{S}_i$ and the conduction-electron spin density

$$\boldsymbol{s}_i \equiv \frac{1}{2} \sum_{\sigma\nu} (c^{\dagger}_{i\sigma} \boldsymbol{\tau}_{\sigma\nu} c_{i\nu})$$

(the three components of $\boldsymbol{\tau}$ are the Pauli matrices, whose components are in turn labelled by σ and ν, and we absorb gyromagnetic ratios and the Bohr magneton in the definition of $\tilde{\boldsymbol{H}}$), $\tilde{J}_H > 0$ is the Hund's-rule coupling, $\tilde{J} < 0$ is the antiferromagnetic superexchange coupling between the localized Mn spins, and $U_0 > 0$ and $U_1 > 0$ are, respectively, on-site and nearest-neighbour Hubbard-repulsion terms. If the orbital angular momentum is fully quenched, the Mn spin has $S = 3/2$. With the localized spins treated as classical, the energy difference between the parallel and antiparallel alignment of the itinerant spin with respect to the localized spin is given by $2\tilde{J}_H S$, which is about $\simeq$3 eV from band calculations [24]. In most of our studies we use the unit cell of the well-known 'CE' structure, a ubiquitous charge- and spin-ordered structure in the manganites observed for $x \simeq 0.5$ [2, 12, 18, 19]. We define the scaled couplings $J \equiv \tilde{J}S^2$, $J_H \equiv \tilde{J}_H S$, and $H \equiv |\tilde{\boldsymbol{H}}|S$, and use the following as typical parameters:

$t \simeq 0.15$ eV
$J_H \simeq 0.75$ eV
$U_0 \simeq 10$ eV
$J \simeq 8$ meV
$U_1 \simeq e^2/(\epsilon r) \simeq 0.3$–$0.4$ eV.

We have studied model (1) via exact diagonalization for finite clusters at $T = 0$ and by a Hartree–Fock mean-field theory at $T \geqslant 0$ for the cubic lattice, which allows for ferromagnetic

(or ferrimagnetic) and antiferromagnetic phases that can be either charge ordered or charge non-ordered. Our studies yield a variety of interesting results which we summarize before giving further details. At $T = 0$ four phases appear: ferromagnetic charge ordered (FO) or charge non-ordered (FN) and antiferromagnetic charge ordered (AFO) or charge non-ordered (AFN). The FO and AFO phases are insulating, whereas the FN and AFN phases are metallic, i.e., metal–insulator transitions in this model are associated with the onset of charge ordering. The energies of these phases are quite close to each other both in our exact, finite-size calculations (figures 1 and 2) and in our mean–field theory (figures 3 and 4); so, by varying parameters such as U_1, x, and H, we can induce (first-order) transitions between them as illustrated in figure 5.

The model accounts for the coupling between charge and spin degrees of freedom, so charge ordering also leads to a change in the magnetic ordering. Small changes in the Hamiltonian parameters can lead to different ground states. For example, at $x = 0.5$ and $T = 0$ (figure 4(b)), we find that, above a critical value of $U_c = U_1/t \simeq 2$, the ground state is AFO, while for lower values, we obtain an FN ground state. Since the estimated value of U_1/t for the manganites is quite close to U_c, our theory offers a natural explanation for why some of these manganites are in the FN phase whereas others are in the AFO phase. Furthermore, figure 4(b) illustrates that, as we increase the bandwidth (by increasing t) at $T = 0$, we stabilize the ferromagnetic phase without charge ordering; conversely, if we lower the bandwidth we stabilize the antiferromagnetic, charge-ordered phase; these trends are in good agreement with experiments [13]. Figures 5(a) and 5(b) show how the band gap and the charge-order parameter jump at the FN–AFO transition at $x = 0.5$ and $T = 0$; note that the band gap is in good agreement with experiments [28].

The phase boundaries at $T = 0$ persist at $T > 0$ and appear as first-order boundaries in a T–μ phase diagram. Since all experimental phase diagrams are shown in the T–x plane, we have converted our T–μ phase diagrams into T–x phase diagrams. Note that first-order boundaries in T–μ phase diagrams correspond to regions of two-phase coexistence in T–x phase diagrams; and a maximum in a first-order phase boundary in the T–μ plane becomes a *point of equal concentration* or *azeotropic point* [30] in the T–x plane. The mean-field phase diagram that we obtain for our model is shown in figures 6 and 7. The AFO phase in our model exists in a narrow range near $x = 1/2$ and also near $x = 0$ or 1. For $x = 1/2$, the AFO phase is bounded on both sides by two-phase coexistence regimes (coexistence of AFO and a weakly charge-ordered FO), which meet at a point of equal concentration at $T = T_{\mathrm{AF}\rightarrow\mathrm{F}}$ ($\simeq$0.03 eV for the parameters of figure 7). The temperature at which this point of equal concentration appears drops rapidly with the magnetic field H as shown in figure 8; this is in agreement with experiments [18, 20]. On further increasing T, the degree of charge ordering in the FO phase increases, until a first-order FO–FN transition occurs at $T \simeq 0.2$ eV, and, at much higher temperatures $T \simeq 1$ eV, a continuous FN–PN transition results as shown in figure 6; here PN stands for an insulating, non-ordered, paramagnetic phase.

There are two effects that should lower the FN–PN transition temperature substantially, namely, (i) the fluctuations neglected in the mean-field theory and (ii) the dynamical Jahn–Teller coupling between electrons and phonons [31, 32], which leads to the isotope effect [33]. The first is a well-known deficiency of the mean-field theories, while, in a recent study, we have shown that the second effect, namely, the dynamical Jahn–Teller coupling, leads to a reduction of the transition temperature by about a factor of three for the manganites [32]. Both of these effects have been omitted in the present theory. Because of this, our calculated T_c for the FN–PN transition is too high as compared to the experimental values.

The remaining part of this paper is organized as follows. In section 2 we describe our exact-diagonalization studies on finite clusters. Section 3 contains our finite-temperature,

mean-field calculations and the results that we obtain from them. Section 4 discusses the experimental implications of our results.

2. Double exchange in extended systems ($T = 0$)

Zener's double-exchange (DEX) mechanism [4] was developed by Anderson and Hasegawa [5] for the case of two atoms, where an itinerant electron moves back and forth between the atoms, each carrying a localized spin S, aligned at an angle θ with respect to each other. They showed that, if the Hund's-rule energy is taken to be infinity, then the effective hopping amplitude is $t\cos(\theta/2)$. This interaction is ferromagnetic and, if strong enough, is sufficient to overcome the AF superexchange between the two atoms, thereby producing a net ferromagnetic interaction.

The DEX ideas can be extended in a straightforward manner to the case of the lattice. But now both the formation of the electron bands and the Coulomb interaction terms must be taken into account. In fact, on general grounds, one may expect the Coulomb interaction to reduce the effect of the DEX interaction, by forcing the electrons to move in a correlated fashion, thereby reducing their kinetic energy. The Coulomb interaction is very important if the number of the itinerant electrons (or holes) is high, and leads to the charge-ordered structures for $La_{1-x}Ca_xMnO_3$ and related systems near half-filling ($x \simeq 1/2$).

To examine the DEX mechanism for an extended system, we have performed an exact-diagonalization study of the ground-state energy for the Hamiltonian (1) for a finite cluster with the magnetic field set equal to zero and by taking a fixed number of electrons. In order to make the calculations tractable, a square lattice was taken and a finite cluster consisting of twelve lattice sites (3×4) with periodic boundary condition was chosen. Here we restrict ourselves to comparing ferromagnetic (F) and Néel antiferromagnetic (AF) arrangements of the localized spins [34]. The (classical) localized spins provide a fixed magnetic background in which the itinerant electrons move. We express the many-electron ground-state as a linear combination of the fermion configurations $|i\rangle$, $|G\rangle = \sum_i \alpha_i |i\rangle$, and obtain it by a numerical diagonalization of the many-electron Hamiltonian via the Lanczos method.

Our results from these exact-diagonalization studies are shown in figures 1 and 2. We have omitted the superexchange term in the figures, i.e., J is set equal to zero. The superexchange energy can be determined quite simply, since the localized spins are treated as classical. Thus, for AF superexchange, the energy of the AF state is reduced with respect to that of the F state by the amount $2J$ times the number of nearest-neighbour bonds, which is of course independent of the number of itinerant electrons in the system. Figure 1 shows the variation of the ground-state energy with the number of electrons N for both F and AF alignments of the localized spins. Our 12-site system can accommodate up to a total of 24 electrons. However, in figure 1, we have only shown the results for up to 12 electrons. The case with more electrons is uninteresting, because the upper Hubbard band that becomes occupied in this case is separated from the lower one by a large energy $\sim(U_0 + J_H)$, and, as a result, it is unlikely to be occupied in the crystal. In the language of the Hubbard model, we consider fillings between 0 and 1/2, which correspond to dopant concentrations x between 0 and 1.

The general trend in the energies in figure 1 can be understood by considering the dominant terms in the Hamiltonian, which are the Hund's-rule term J_H and the nearest-neighbour Coulomb interaction term U_1. The former contributes an energy $-J_H \times N$, where N is the total number of electrons; this arises because of the filling of the electron states with spins aligned parallel to the localized spins. When the average electron density n becomes greater than one half-electron per site, the addition of an electron raises the energy on average by an amount zU_1 because of the nearest-neighbour Coulomb term (z, the number of nearest neighbours, is 4 for the square lattice). Thus, these two terms lead to the energy $E = -J_H N$ if

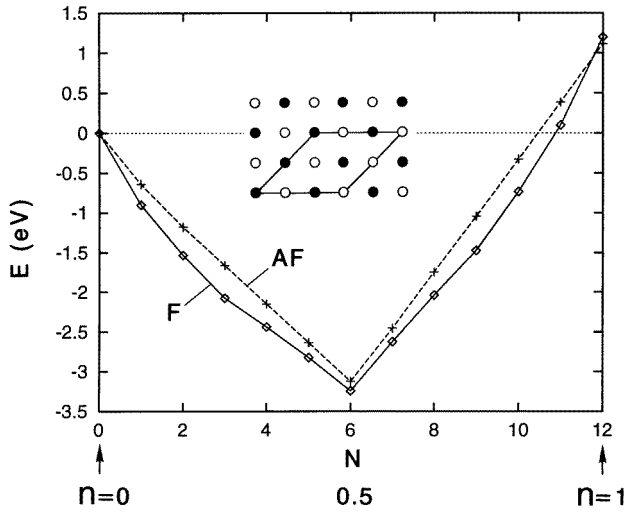

Figure 1. Energies of the ferromagnetic (F) and antiferromagnetic Néel (AF) states obtained from exact diagonalization on a 12-site (3×4) cluster on a square lattice. The inset shows the ordered AF lattice of the $Mn_{t_{2g}}$ spins and the unit cell used with periodic boundary conditions. N is the total number of electrons and $n = N/12$ is the electron density per site. The Hamiltonian parameters are: $U_0 = 5$ eV, $U_1 = 0.3$ eV, $t = -0.1$ eV, and $J_H = 0.25$ eV. Also, here $J = 0$. A finite antiferromagnetic J shifts the energy of the AF state down with respect to that of the F state by a fixed amount, irrespective of N.

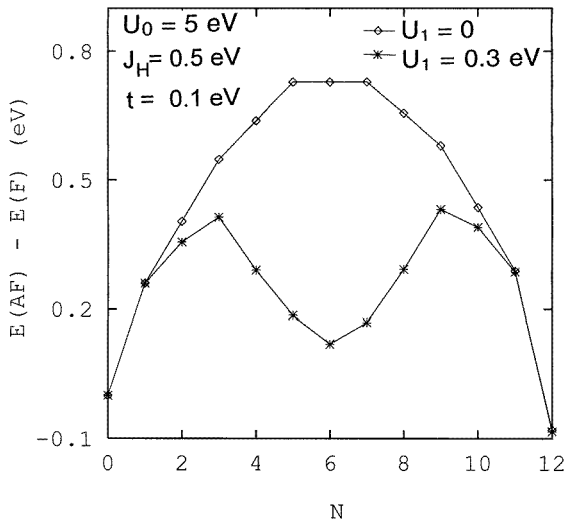

Figure 2. Double-exchange energy, obtained by taking the energy difference between the AF and the F states of figure 1 for two different values of U_1. Individual points are joined by lines to guide the eye. Note the significant reduction of the double-exchange energy near $n = 1/2$ for the case of $U_1 \neq 0$, caused by the reduction of the kinetic energy due to Coulomb correlation produced by the nearest-neighbour Coulomb term.

$N \leqslant 6$ and $E = -J_H N + 4U_1(N - 6)$ if $6 \geqslant N \geqslant 12$ ($N = 6$ corresponds to the filling factor of one electron per Mn site). This trend is very clearly seen in figure 1. In addition to this,

for both AF and F structures, there is a gain in the kinetic energy, but this gain is significantly higher for the F state because of the double-exchange interaction, so the total energy of the F state is always lower than that of the AF state. Note that we have set $J = 0$ in figure 1. Now, for an antiferromagnetic superexchange J, the energy for the AF state in figure 1 is reduced by a fixed amount with respect to that of the F state. If J is very large, the system is always AF, the DEX interaction being insufficient to induce ferromagnetism in the system. If J is small, then there exists a range of concentration x where the system is ferromagnetic, and a range where it is antiferromagnetic.

The energy difference between the AF and the F states is shown in figure 2. We see that, even though the F state is energetically favoured over the AF state, for $n \simeq 1/2$, the double-exchange gain of energy is considerably diminished. This shows clearly that the nearest-neighbour Coulomb interaction U_1 has an important effect in this range. To illustrate the point further, we have performed a separate calculation with identical Hamiltonian parameters except for U_1 which we now choose to be zero; the energy difference between AF and F states does not show a dip for $n \simeq 1/2$ in this case (figure 2). Instead, for $U_1 = 0$, we obtain the result that might be expected—namely, that the larger the number of the itinerant carriers (electrons or holes), the stronger the double-exchange energy gain. This clearly shows how the nearest-neighbour Coulomb interaction competes with the double-exchange mechanism especially for $n \simeq 1/2$. We will show in the next section that the former is also crucial in stabilizing charge-ordered phases near $x = 1/2$.

Exact-diagonalization calculations are only feasible for small clusters of sites. All of our studies on the infinite, three-dimensional lattices reported in this paper are performed with mean-field (Hartree or Hartree–Fock) methods. In view of the fact that the spin-flip terms may be present in the Hamiltonian (e.g., if spin-quantization axes are chosen differently for different atoms), the terms containing expectation values of spin-flip operators such as $\langle c^{\dagger}_{i-\sigma} c_{j\sigma} \rangle$ in the HF approximation must now be retained. Thus the HF approximation for the NN Coulomb interaction term is given by the expression

$$U_1 \sum_{\sigma\sigma'} \hat{n}_{1\sigma}\hat{n}_{2\sigma'} = U_1[\langle \hat{n}_1 \rangle \hat{n}_2 + \hat{n}_1 \langle \hat{n}_2 \rangle - \sum_{\sigma} c^{\dagger}_{2\sigma} c_{1\sigma} \langle c^{\dagger}_{1\sigma} c_{2\sigma} \rangle + c^{\dagger}_{1\sigma} c_{2\sigma} \langle c^{\dagger}_{2\sigma} c_{1\sigma} \rangle - \sum_{\sigma} c^{\dagger}_{2\sigma} c_{1-\sigma} \langle c^{\dagger}_{1-\sigma} c_{2\sigma} \rangle + c^{\dagger}_{1\sigma} c_{2-\sigma} \langle c^{\dagger}_{2-\sigma} c_{1\sigma} \rangle]. \tag{2}$$

Before describing our finite-temperature mean-field theory (section 3) we wish to point out that, at $T = 0$, the competition between the double-exchange and nearest-neighbour Coulomb terms mentioned above also emerges from a mean-field approximation.

To this end, we have calculated the total energies for the F and the Néel AF (also called the 'type-G' structure) states for model (1) on a simple-cubic lattice by using the self-consistent Hartree–Fock (HF) method. The HF results (figure 3), show the same qualitative trend as found in our exact-diagonalization study—namely, that the energy difference between the F and AF states is smallest near $n \simeq 1/2$ because of the nearest-neighbour Coulomb interaction.

Notice that near $x = 1$, the energy of the AF state is somewhat *lower* than that of the F state in both the exact-diagonalization and the Hartree–Fock results (figures 1 and 3). This can be shown to be due to hybridization with the upper Hubbard band in the model. This illustrates an important point—namely, that hybridization with energetically higher bands in the system can reverse the DEX interaction to favour antiferromagnetism. Such considerations may be important in understanding the AF state in $La_{1-x}Ca_xMnO_3$ for the range of dopant concentration $x > 0.5$.

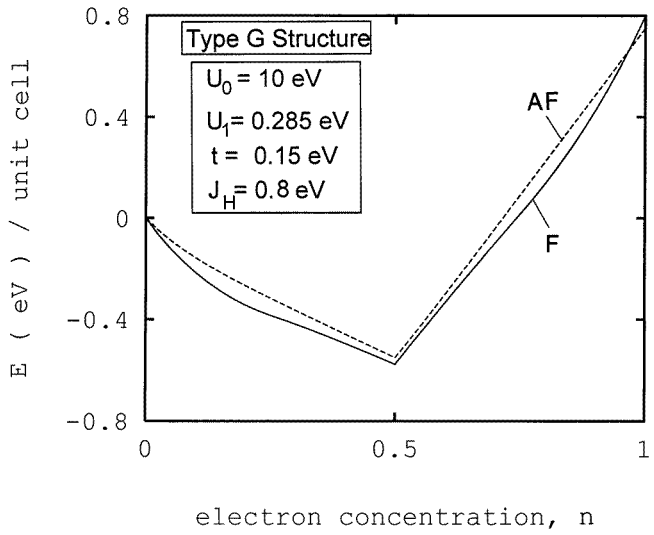

Figure 3. Energies of the F and the Néel AF states for the simple-cubic lattice (type-G structure) obtained from the self-consistent Hartree–Fock calculation. The superexchange term J is taken to be zero.

3. Mean-field calculations at $T \geqslant 0$

For $T \geqslant 0$ we have studied model (1) by using a mean-field (Hartree) approximation [35]. Specifically we use a Gibbs–Bogoliubov–Peierls variational principle [36] in which we write

$$\mathcal{H} = \mathcal{H}_{quas} + \mathcal{H}_{fluc} \tag{3}$$

where the subscripts stand for quasiparticle and fluctuation, respectively;

$$\begin{aligned}\mathcal{H}_{quas} = &-t \sum_{\langle ij\rangle,\sigma} c^{\dagger}_{i\sigma} c_{j\sigma} - (\mu + \tilde{J}_H \mathcal{M}^z_i - \tilde{H}) \sum_i \hat{n}_{i\uparrow} - (\mu - \tilde{J}_H \mathcal{M}^z_i + \tilde{H}) \sum_i \hat{n}_{i\downarrow} \\ &+ U_0 \sum_i (\hat{n}_{i\uparrow} f_{i\downarrow} + \hat{n}_{i\downarrow} f_{i\uparrow}) + U_1 \sum_{i,\sigma\nu} \left(\hat{n}_{i\sigma} \sum_j{}' (f_{j\nu}) \right) \\ &- \sum_i \left(\tilde{H} + \tilde{J} \sum_j{}' \mathcal{M}^z_j + \tilde{J}_H (f_{i\uparrow} - f_{i\downarrow}) \right) S^z_i \\ &- U_0 \sum_i f_{i\uparrow} f_{i\downarrow} - U_1 \sum_{\langle ij\rangle,\sigma\nu} f_{i\sigma} f_{j\nu} \\ &+ \tilde{J} \sum_{\langle ij\rangle} \mathcal{M}^z_i \mathcal{M}^z_j + \tilde{J}_H \sum_i \mathcal{M}^z_i (f_{i\uparrow} - f_{j\downarrow}).\end{aligned} \tag{4}$$

Here $\sum'_j$ denotes a sum over all sites j that are nearest neighbours of i, and we have allowed magnetic ordering in the direction of $\tilde{\boldsymbol{H}}$ (henceforth the z-direction). $\mathcal{H}_{fluc}$ follows from equations (1), (3), and (4). The variational parameters $f_{i,\sigma}$ and $\mathcal{M}^z_i$ are determined by minimizing a variational grand potential Ω_{var} discussed below. The minimum of Ω_{var} is achieved [36] when these parameters are equal to the charge and magnetization densities [37], respectively, which satisfy self-consistency conditions. Finally the magnetic order parameters

$M_i \equiv \langle \boldsymbol{S}_i \rangle$ satisfy the self-consistency equations

$$M_i = B_S\left(\beta\left(J\sum_j{}' M_j + J_H m_i + H\right)\right) \tag{5}$$

where $\beta \equiv (k_B T)^{-1}$, k_B is the Boltzmann constant, the prime on the sum denotes nearest neighbours of site i, the spin density $m_i \equiv \langle \hat{n}_{i\uparrow} - \hat{n}_{i\downarrow} \rangle$, and B_S is the Brillouin function, for $S = 3/2$. Furthermore, we write the Hamiltonian $\mathcal{H}_{quas}$ (equation (4)) in Fourier space using Bloch symmetry and then diagonalize the resulting Hamiltonian matrix for each point in the Brillouin zone (for the CE structure, we have a 32×32 matrix, there being 16 sites in the unit cell). The charge densities $n_{i\sigma} \equiv \langle \hat{n}_{i\sigma} \rangle$ are determined self-consistently from the eigenvectors of the effective mean-field Hamiltonian. For the CE structure and with $H = 0$, there are a total of six order parameters in our model—namely, M_i, m_i, and $n_i = \langle n_{i\uparrow} + n_{i\downarrow} \rangle$, with $i = \circ$ or $i = \bullet$ being the two types of Mn site in the CE structure with nominal valence Mn^{4+} and Mn^{3+}, respectively. For $H > 0$, in total twelve order parameters are required. We solve our self-consistency conditions by a numerical iteration scheme [38]. These equations have many solutions, so we start our iteration scheme with as many as 60 initial guesses and, if we find multiple solutions, which we occasionally do for parameters close to the phase transition regions, we pick the one which yields the lowest value of the variational grand potential [36,37] per cell:

$$\begin{aligned}\Omega_{var} = {} & -8U_0(n_{\bullet\uparrow}n_{\bullet\downarrow} + n_{\circ\uparrow}n_{\circ\downarrow}) - 8U_1(n_\bullet^2 + n_\circ^2 + 4n_\bullet n_\circ) \\ & + 8J(4M_\bullet M_\circ + M_\bullet^2 + M_\circ^2) + 8J_H[M_\bullet(n_{\bullet\uparrow} - n_{\bullet\downarrow}) + M_\circ(n_{\circ\uparrow} - n_{\circ\downarrow})] \\ & - \frac{T}{N_k}\sum_{\boldsymbol{k}} \ln[1 + \exp(-\beta\omega(\boldsymbol{k})] - 4T\sum_{i=\bullet,\circ} \ln\frac{\sinh(\beta H_i^{eff}(2S+1)/(2S))}{\sinh(\beta H_i^{eff}/(2S))}.\end{aligned} \tag{6}$$

Here N_k is the number of k-points that we use in summing over the Brillouin zone, $\omega(\boldsymbol{k})$ are the eigenvalues obtained by diagonalizing the 32×32 matrix at each $\boldsymbol{k}$-point, and H_i^{eff}, the effective fields at sites i ($=\bullet, \circ$), are

$$\begin{aligned} H_\bullet^{eff} &\equiv J(4M_\circ + 2M_\bullet) + J_H(n_{\bullet\uparrow} - n_{\bullet\downarrow}) \\ H_\circ^{eff} &\equiv J(4M_\bullet + 2M_\circ) + J_H(n_{\circ\uparrow} - n_{\circ\downarrow}). \end{aligned} \tag{7}$$

Note that in the CE structure, each Mn site is surrounded by four sites of its own kind ($\bullet$ or $\circ$) and two of the other kind. Note also that throughout this paper, the dopant concentration x is related to the electron concentration n by the expression $x = 1 - n$, where both vary between 0 and 1. If we choose to work with a fixed density n, which is especially convenient at $T = 0$, we must minimize $\Omega_{var} + \mu n$, which becomes the energy E_{var} per unit cell at $T = 0$.

We begin with our mean-field results at $T = 0$, which are shown in figures 4 and 5 for the 'CE' structure. The energies of the F and the AF phases are shown in figure 4(a) as a function of the dopant concentration x. With the parameters chosen, the two phases are very close in energy, and therefore the system can show transitions from one phase into another on the application of heat or magnetic field or upon slight change of the Hamiltonian parameters. The energies for the F and the AF phases are shown in figure 4(b) as a function of U_1 for $x = 1/2$. The phase with the lowest energy is the equilibrium phase. As seen from the figure, depending on the magnitude of U_1, either a charge-ordered or a charge-non-ordered phase results. Figure 4(c) shows how the equilibrium phase 'melts' from the AFO to the FN phase on application of a magnetic field.

We note the following points from figures 4 and 5:

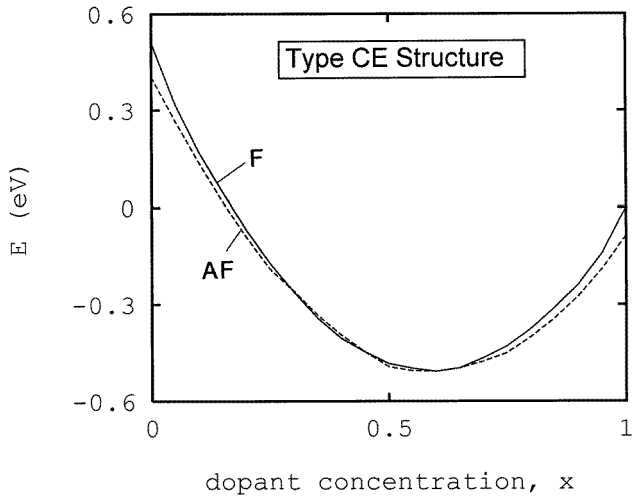

(a)

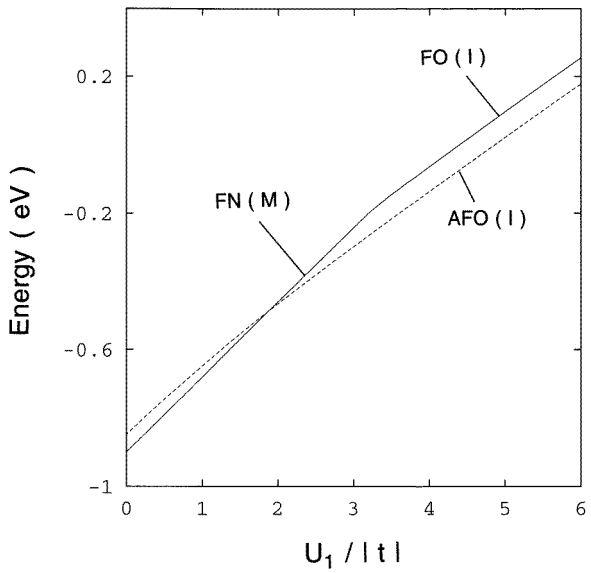

(b)

Figure 4. (a) The variations of the $T = 0$ mean-field energies of the ferromagnetic and antiferromagnetic (CE structure) states with x. The parameters are: $U_0 = 10$ eV, $U_1 = 0.285$ eV, $t = 0.15$ eV, $J = 10$ meV, and $J_H = 0.8$ eV. The energies are per two Mn sites in the lattice. (b) The variation of the energies of the ferromagnetic and antiferromagnetic (CE) structures at $T = 0$ with the nearest-neighbour Coulomb repulsion U_1 at $x = 1/2$. (c) The variation of the energies of the ferromagnetic and antiferromagnetic phases illustrating the 'melting' of the charge-ordered antiferromagnet into a charge-non-ordered ferromagnet induced by an applied magnetic field H.

(1) Charge ordering is favoured by large U_1, so by increasing U_1 we can induce an FN–AFO transition.

(2) The charge-ordered AFO phase can be 'melted' by the application of a weak magnetic field as in experiments [18, 20].

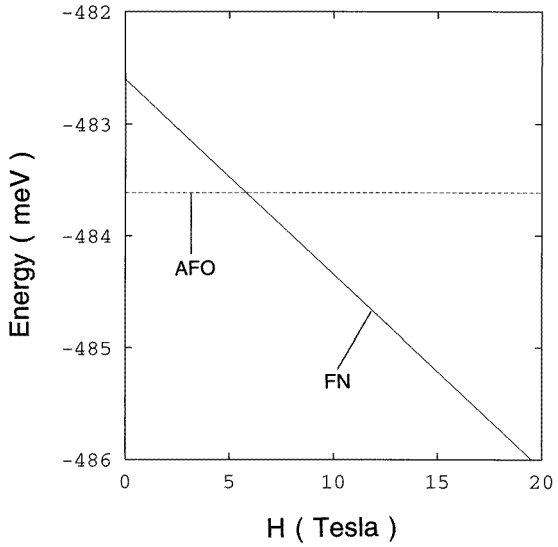

(c)

Figure 4. (Continued)

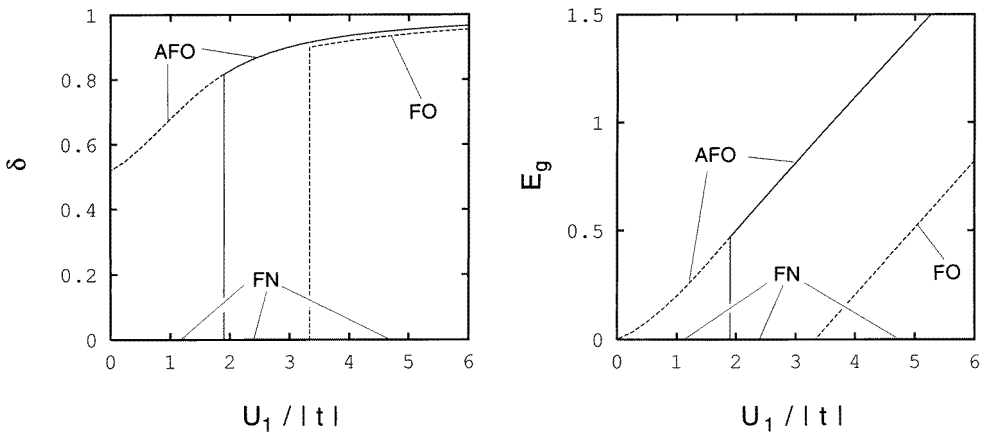

(a) (b)

Figure 5. Variations of (a) the charge-order parameter δ and (b) the one-particle gap E_g with U_1 for the data of figure 4(b). The one-particle gaps were obtained from calculating the electronic band structure at a large number of k-points in the irreducible Brillouin zone.

(3) The FN–AFO transition is first order as can be seen from the jumps in the charge-order parameter and band gap in figure 5. Note, in particular, that the gap that we get in the AFO phase is comparable to the charge-ordering gaps found in experiments [28].

(4) Figure 4(b) also illustrates that, as we increase the bandwidth by increasing t, we stabilize the ferromagnetic phase without charge ordering; but, if we lower the bandwidth, we stabilize the antiferromagnetic, charge-ordered phase; this trend has been seen in experiments [13].

Figures 4(b) and 5(a), 5(b) therefore show a simultaneous, first-order phase transition from a ferromagnetic to antiferromagnetic, charge-ordered to charge-non-ordered, and metal-to-insulator transition as U_1 is varied.

When considering plots like figure 4(b), one must, of course, make a Maxwell construction, if necessary, to obtain a properly convex energy; our grand-canonical calculations at $T \geqslant 0$ account for this. Note also that the precise structure of the unit cells in different members of the family $Ln_{1-x}A_xMnO_3$ could be different from the CE structure that we consider here. We have not tried to include all of these possible structures in our variational calculation, since we principally wish to illustrate the *essential mechanism* for charge ordering in this class of compounds.

We have seen above that, by changing the Hamiltonian parameters, we can stabilize different phases at $T = 0$. Thus different sets of values for the parameters in our model can lead to different topologies of phase diagrams at $T > 0$. It is most convenient to work in the grand-canonical ensemble in which the filling, i.e., x, depends on T and μ. If μ is large and negative, $x \simeq 1$, but if μ is large and positive, $x \simeq 0$. We first obtain our mean-field phase diagram for model (1) in the T–μ plane and then obtain the corresponding T–x phase diagram.

Figure 6 shows qualitatively the phase diagram that we obtain from our model, where, in addition to the CE structure relevant for $x \simeq 0.5$, we have also considered the 'type-A' and 'type-G' structures, relevant for the concentrations $x \simeq 0$ and $x \simeq 1$, respectively. In figure 7 we show the details of the phase diagram close to $x = 0.5$. The salient features of our mean-field phase diagram are as follows. At low T it has antiferromagnetic phases near $x \simeq 0$ and $x \simeq 1$ as in experiments; the antiferromagnetic charge-ordered phase (AFO) appears in the vicinity of $x = 1/2$; given the parameter values that we use, a weakly charge-ordered ferromagnet (FO) is stabilized at low T (it loses its charge ordering as $T \to 0$). The AFO–FO transition is first order; this leads to the two-phase regions shown in figure 7. They come together at a point of equal concentration or azeotropic point.

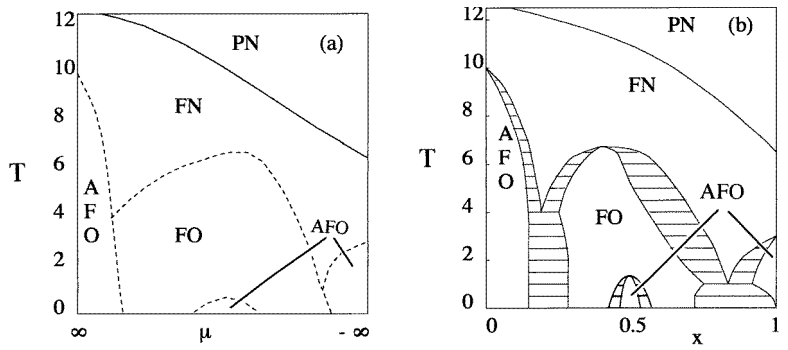

Figure 6. Sketches of the global (a) T–μ and (b) T–x phase diagrams suggested from our model by examining several crystal structures in addition to the CE structure. The temperature T is in units of k_B/t. The height of the central AFO phase is exaggerated to make it visible (see figure 7 for the correct scales).

It is worth mentioning that an important feature of the phase diagram of the manganites in the electron-doped region—namely, that $La_{1-x}Ca_xMnO_3$ is antiferromagnetic over the entire range of $0.5 \leqslant x \leqslant 1$—is not reproduced from the one-band model, which we have studied here. In the standard Anderson–Hasegawa double exchange, it is immaterial whether we have electrons or holes as carriers. This is manifested in our model as a roughly symmetrical phase diagram about $x = 1/2$ (figures 6 and 7), which is not seen in the experiments. This issue is

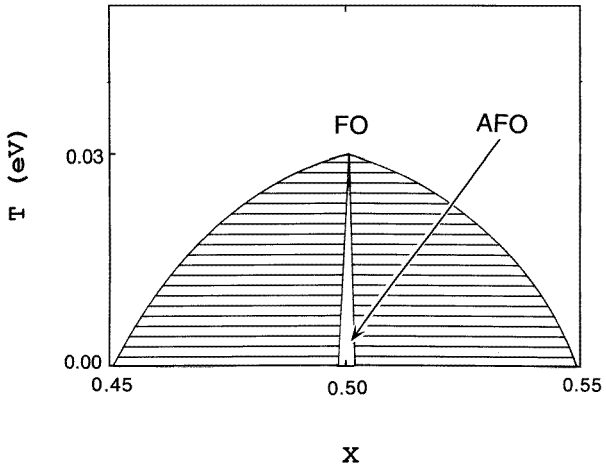

Figure 7. The phase diagram obtained from our model near $x = 0.5$. The CE structure has the lowest free energy in this region. The hatched areas are regions of two-phase (AFO + FO) coexistence, which come together at a point of equal concentration or azeotropic point at $x = 1/2$, and $T = T_{\mathrm{AF}\rightarrow\mathrm{F}}$ (the sharpness of this point in our figure is an artifact of the finite graphical resolution). The parameters are: $U_1 = 0.285$ eV, $U_0 = 10$ eV, $t = 0.15$ eV, $J_H = 0.8$ eV, and $J = 10$ meV.

not addressed in any theoretical work to our knowledge. We think that a multi-band model that includes not only the e_g orbitals, but also the higher-lying, unoccupied t_{2g} orbitals of spins opposite to the core t_{2g} spins, will be an important ingredient in determining the phase diagram in the electron-doped regions. It is easy to see that hopping between the e_g orbital and the higher-lying t_{2g} orbital will produce a non-standard *anti*ferromagnetic DEX interaction between the core t_{2g} levels of neighbouring Mn atoms.

If we carry out our calculation in the presence of an external magnetic field, then the temperature $T_{\mathrm{AF}\rightarrow\mathrm{F}}$, at which this point of equal concentration occurs, drops rapidly with H as shown in figure 8. This is in accord with experiments [18, 20] which have reported the 'melting' of the charge-ordered antiferromagnet on the application of a weak magnetic field. Note that, given our parameters, the field required to reduce $T_{\mathrm{AF}\rightarrow\mathrm{F}}$ to zero is comparable to that found in experiments.

The behaviour of the charge-order parameter, defined as the difference between the charges on the two sublattices, $\delta \equiv n_\bullet - n_\circ$, as a function of T (at fixed $x = 1/2$) and as a function of x (at fixed $T = 0.015$ eV) is shown, respectively, in figures 9 and 10 for $H = 0$; these illustrate the first-order nature of the AFO–FO transition. In obtaining figure 10 we have used the lever rule to compute the order parameter δ in the two-phase regions. Note that near $x = 1/2$, the pure AFO phase is stable only in a very narrow region of x, and that our phase diagram is roughly symmetrical about $x = 1/2$. We will return to a discussion of this symmetry and the two-phase coexistence regimes in section 4.

Our zero-temperature FN phase (figure 4(c)) evolves smoothly at finite T into an FO phase (figure 8) with weak charge ordering. It would have been ideal, from the point of view of experiments, which normally obtain a ferromagnetic metallic phase (i.e., our FN) above the AFO phase, if this weak charge ordering had been absent in our model (at least at the level of our mean-field theory). However, it is worth noting that charge-ordered insulating phases are observed above low-T antiferromagnets in some systems such as $Pr_{1-x}Ca_xMnO_3$ (see figure 21 of reference [13]). To the extent that our model does not include all physically

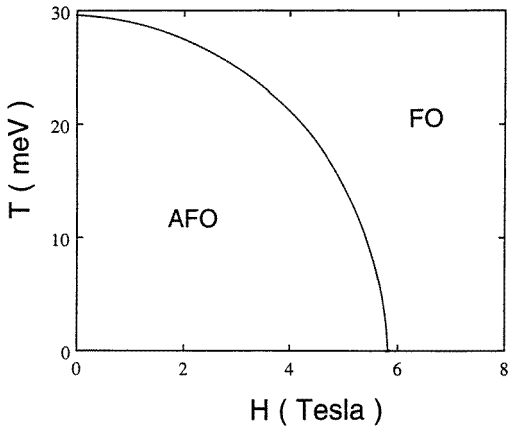

Figure 8. The drop in $T_{\mathrm{AF}\to\mathrm{F}}$, the temperature at which the point of equal concentration occurs in figure 7, with magnetic field H. The AFO phase at low H melts to an FO phase as H increases. There is a large jump in the charge-order parameter across the phase boundary, since the FO phase turns out to have only a small degree of charge ordering, which actually goes to zero as $T \to 0$.

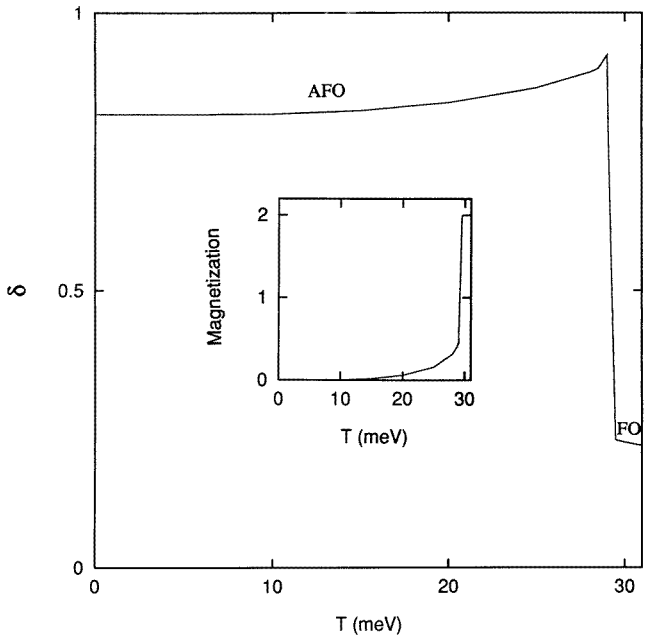

Figure 9. The variation of the charge-order parameter δ and the magnetization M (inset) with temperature T illustrating the AFO–FO transition at the point of equal concentration at $x = 1/2$ corresponding to figure 7.

relevant interactions like electron–phonon couplings, some of its predictions (e.g., weak charge ordering in the finite-T FO phase) should be viewed as illustrating possible types of phase in this class of systems.

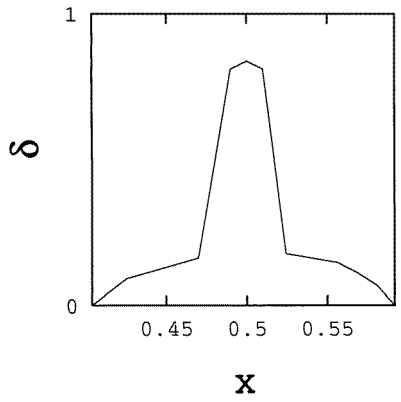

Figure 10. The variation of the charge-order parameter δ with dopant concentration x at a fixed temperature $T = 0.015$ eV corresponding to figure 7.

4. Conclusions

We have presented a model for the CMR manganites which captures the competition between double-exchange and superexchange interactions. The extended-Hubbard term in our model is crucial for the metal–insulator transitions that are associated with the loss of charge ordering seen in the experiments [15, 16, 20]. The magnetic field dependence of this transition is also in good accord with experiments [18, 20]. Thus our work, which complements other theoretical studies [39–43], elucidates the nature of charge ordering in CMR manganites. A complete theory of these materials must, of course, integrate these effects with those caused by electron–phonon interactions, disorder, and orbital ordering. Before discussing this issue, we discuss the experimental implications of some of our results.

Experiments are done at a fixed value of x. If, at some T, x lies in a region of two-phase coexistence, phase separation should occur and the equilibrium state should consist of two phases separated by an interface. The equilibrium values of x in these coexisting phases are given by the boundaries of the coexistence curve at that value of T. Such an equilibrium state might be hard to obtain in experiments on the CMR manganites since dopant-atom diffusion might be kinetically hindered. Furthermore, data analysis may be complicated by the possible presence of multiple intermediate phases [44] and oxygen stoichiometry issues. Note that the mere inclusion of long-range Coulomb interactions in our model will not suppress two-phase coexistence regimes of the type shown in figures 6 and 7. These coexistence regimes will be suppressed *only if, in addition,* the dopant atoms do not phase separate, leading to a net charge imbalance between the coexisting phases. It is also possible that long-range Coulomb interactions might lead to the stabilization of phases with complicated ordering such as an incommensurate (or disordered) phase, consisting of small insulating regions in a metallic background or vice versa. The investigation of such orderings lies beyond the scope of our study. On the experimental side, evidence for phase separation has been seen in several recent experiments on the CMR samples. For example, from neutron measurements on samples of $La_{0.53}Ca_{0.47}MnO_3$, Rhyne *et al* [45] have found the coexistence of a ferromagnetic and an antiferromagnetic phase, and Roy *et al* have found the same from electrical conductivity measurements [46]. A similar two-phase coexistence has also been recently reported for the (La, Pr, Ca)MnO_3 system [47].

We have restricted our study mostly to one type of antiferromagnetic ordering and one

type of lattice—namely, the CE structure—since our principal goal in this paper is to illustrate the mechanism of charge ordering. To obtain correct structures and changes to the structure at these transitions, or charge-ordered phases interpreted as polaronic crystals [48], we must of course include other interactions. By virtue of using a single-band model, motivated by the Jahn–Teller splitting of the e_g band in $LaMnO_3$, we have implicitly accounted for some degree of electron–phonon interactions; clearly a more detailed modelling of these interactions is required to obtain charge-ordered phases that can be interpreted as polaronic crystals. We note that, once charge ordering sets in because of the repulsion term U_1, it will induce a Jahn–Teller-type frozen-phonon distortion, i.e., a polaronic crystal. Also further-neighbour superexchange terms, that should destabilize other phases like a conventional two-sublattice antiferromagnet, might well have to be included to make the CE structure the most stable one near $x = 1/2$. But then one should use a multi-band model and perhaps also different values for in-plane and out-of-plane hopping amplitudes, in view of the in-plane orientation of the $e_g^{(1)}$ orbital and orbital ordering [24, 49, 50]. Indeed, such models might well be required to remove the near symmetry about $x = 1/2$ in our phase diagram (figure 7), which is not seen in experiments.

Our paramagnetic phase is metallic, though in experiments it is normally insulating, even away from commensurate fillings. Clearly disorder effects (both spin disorder [51] and disorder arising from doping) must be included to make the AFO and PN phases insulating away from half-filling. Furthermore, the FO–FN and FN–PN transition temperatures T_c are far too high in our mean-field theory. This is not surprising, for it is well known that the Hartree–Fock estimate for the antiferromagnet–paramagnet transition in the half-filled Hubbard model is far too high (of the order of the on-site repulsion U rather than of the order of $|t|^2/U$ at large U). Fluctuations neglected in our mean-field theory must therefore be included to get a more reasonable estimate for the FN–PN transition temperature. However, it is not clear yet how to use other approximations (like Schwinger-boson mean-field theories [52, 53] or infinite-dimensionality methods [54]) for a model as complex as ours. An additional effect that would reduce this T_c is the dynamical Jahn–Teller coupling between the electrons and phonons, which has its physical origin in the fact that, as the electron moves from site to site, it has a tendency of carrying the Jahn–Teller distortion around the Mn^{3+} octahedron along with it. The quantum-mechanical nuclear wave function of the oxygen atom becomes involved, and, as a consequence, the double exchange is diminished by a factor estimated to be as large as three [31, 32].

In summary, we have studied theoretically the competition between charge-ordered and other magnetically ordered phases in the CMR manganites. Our study indicates the crucial role of electron–electron interactions in stabilizing the charge order observed in the manganites. Furthermore, we obtain from our study the two-phase coexistence region between AFO and FO phases near $x = 1/2$, consistent with evidence obtained from recent experiments.

Acknowledgments

This work was supported in part by the Office of Naval Research under contract No ONR N00014-95-1-0439. One of us (RP) thanks the Department of Physics, University of Missouri–Columbia for hospitality, during the time that this work was done, and UGC (India). We thank F Aryasetiawan, O Gunnarsson, C Jayaprakash, H R Krishnamurthy, R Mahendiran, T V Ramakrishnan, C N R Rao, A K Raychaudhuri, J Rhyne, and D D Sarma for valuable discussions.

References

[1] Jonker G H and Van Santen J H 1950 *Physica* **16** 337
Jonker G H and Van Santen J H 1950 *Physica* **16** 599
[2] Wollan E O and Koehler W C 1955 *Phys. Rev.* **100** 545
[3] Goodenough J B 1955 *Phys. Rev.* **100** 564
[4] Zener C 1951 *Phys. Rev.* **82** 403
[5] Anderson P W and Hasegawa H 1955 *Phys. Rev.* **100** 675
[6] de Gennes P-G 1960 *Phys. Rev.* **118** 141
[7] von Helmolt R, Weckberg J, Holzapfel B, Schultz L and Samwer K 1993 *Phys. Rev. Lett.* **71** 2331
[8] Chahara K, Ohno T, Kasai M and Kozono Y 1993 *Appl. Phys. Lett.* **63** 1990
[9] Jin S, Tiefel T H, Fastnacht R A, Ramesh R and Chen L H 1994 *Science* **264** 413
[10] Ju H L, Kwon C, Li Q, Greene R L and Venkatesan T 1994 *Appl. Phys. Lett.* **65** 2108
[11] Okimoto Y, Katsufuji T, Ishikawa T, Urushibara A, Arima T and Tokura Y 1995 *Phys. Rev. Lett.* **75** 109
[12] Mahendiran R, Mahesh R, Raychaudhuri A K and Rao C N R 1995 *J. Phys. D: Appl. Phys.* **28** 1743
[13] Rao C N R, Cheetham A K and Mahesh R 1996 *Chem. Mater.* **8** 2421
[14] Ramirez A P 1997 *J. Phys.: Condens. Matter* **9** 8171
[15] Troyanchuk I O 1992 *Zh. Eksp. Teor. Fiz.* **102** 251 (Engl. Transl. 1992 *Sov. Phys.–JETP* **75** 132)
[16] Schiffer P, Ramirez A P, Bao W and Cheong S-W 1995 *Phys. Rev. Lett.* **75** 3336
[17] Verwey E J W, Haayman P W and Romeijn F C 1947 *J. Chem. Phys.* **15** 181
[18] Kuwahara H, Tomioka Y, Asamitsu A, Moritomo Y and Tokura Y 1995 *Science* **270** 961
[19] Kawano H, Kajimoto R, Yoshizawa H, Tomioka Y, Kuwahara H and Tokura Y 1997 *Phys. Rev. Lett.* **78** 4253
[20] Tomioka Y, Asamitsu A, Morimoto Y, Kuwahara H and Tokura Y 1995 *Phys. Rev. Lett.* **74** 5108
[21] Knizek K, Jirak Z, Pollert E, Zounova F and Vratislav S 1992 *J. Solid State Chem.* **100** 292
Tomioka Y, Asamitsu A, Kuwahara H, Morimoto Y and Tokura Y 1996 *Phys. Rev.* B **53** R1689
[22] Cullen J R and Callen E R 1973 *Phys. Rev.* B **7** 397
[23] Mishra S K, Zhang Z and Satpathy S 1994 *J. Appl. Phys.* **76** 6700
[24] Satpathy S, Popović Z S and Vukajlović F R 1996 *Phys. Rev. Lett.* **76** 960
[25] Pickett W E and Singh D J 1996 *Phys. Rev.* B **53** 1146
[26] Sarma D D, Shanthi N, Barman S R, Hamada N, Sawada H and Terakura K 1995 *Phys. Rev. Lett.* **75** 1126
[27] Several results for this model were reported by us in:
Mishra S K, Pandit R and Satpathy S 1997 *Phys. Rev.* B **56** 2316
[28] Biswas A, Raychaudhuri A K, Mahendiran R, Guha A, Mahesh R and Rao C N R 1997 *J. Phys.: Condens. Matter* **9** L355
These authors obtain a charge-ordering gap of $\simeq$0.27 eV in $Nd_{0.5}Sr_{0.5}MnO_3$ below the charge-ordering temperature. In other related compounds the charge-ordering gap lies in the range 0.25–0.6 eV [29]; see also:
Chainani A, Kumigashira H, Takahashi T, Tomioka Y, Kuwahara H and Tokura Y 1997 *Preprint* Tohoku University
[29] Arulraj A, Biswas A, Raychaudhuri A K, Rao C N R, Cheetham A K, Woodward P M, Vogt T and Cox D E 1998 *Phys. Rev.* B **57** R8115
[30] Landau L D and Lifshitz E M 1977 *Statistical Physics* (New York: Pergamon) p 307
[31] Kresin V Z and Wolf S A 1997 *Phil. Mag.* B **76** 241
[32] Satpathy S 1998 *J. Phys.: Condens. Matter* **10** L501
Meskine H and Satpathy S 1999 *J. Appl. Phys.* **85** 4348
Satpathy S 1999 *Solid State Commun.* at press
[33] Zhao G-M, Conder K, Keller H and Müller K A 1996 *Nature* **381** 676
Franck J P, Isaac I, Chen W, Chrzanowski J and Irwin J C 1998 *Phys. Rev.* B **58** 5189
[34] In an earlier work, we examined the case of canted classical spins in connection with the manganites from an exact-diagonalization study. See:
Mishra S K, Satpathy S, Aryasetiawan F and Gunnarsson O 1997 *Phys. Rev.* B **55** 2725
[35] We restrict ourselves to the Hartree approximation for the complicated CE structure. We have checked for simpler structures that Hartree and Hartree–Fock approximations give similar results.
[36] Girardeau M and Mazo R 1973 *Advances in Chemical Physics* vol 24, ed I Prigogine and S A Rice (New York: Wiley) pp 187–255
[37] The Gibbs–Bogoliubov–Peierls variational principle states [36] that $\Omega \leqslant \Omega_{var} + \langle \mathcal{H}_{fluc} \rangle_0$, where the subscript 0 indicates that the thermal average is evaluated by using $\mathcal{H}_{quas}$ as the Hamiltonian. Since $f_{i\sigma} = n_{i,\sigma}$, etc, at the minimum, $\langle \mathcal{H}_{fluc} \rangle_0 = 0$, so we merely have to minimize Ω_{var} (equation (6)).

[38] Our convergence criterion is that the sum of the squares of the differences between successive iterates of our six order parameters is less than 10^{-6}.
[39] Furukawa N 1994 *J. Phys. Soc. Japan* **63** 3214
Furukawa N 1995 *J. Phys. Soc. Japan* **64** 2734
Furukawa N 1995 *J. Phys. Soc. Japan* **64** 3164
[40] Millis A J, Littlewood P B and Shraiman B I 1995 *Phys. Rev. Lett.* **74** 5144
[41] Millis A J, Shraiman B I and Mueller R 1996 *Phys. Rev. Lett.* **77** 175
[42] Inoue J and Maekawa S 1995 *Phys. Rev. Lett.* **74** 3407
[43] Malvezzi A L, Yunoki S and Dagotto E 1999 *Phys. Rev.* B **59** 7033
[44] Radaelli P G, Cox D E, Marezio M, Cheong S-W, Schiffer P E and Ramirez A P 1995 *Phys. Rev. Lett.* **75** 4488
[45] Rhyne J J, Kaiser H, Luo H, Xiao G and Gardel M L 1998 *J. Appl. Phys.* **83** 7339
[46] Roy M, Mitchell J, Ramirez A P and Schiffer P 1998 *Phys. Rev.* B **58** 5185
[47] Uehara M, Cheong S-W, Chen C H and Mori S 1999 *Bull. Am. Phys. Soc.* **44** 654
[48] Yamada Y, Hino O, Nohdo S, Kanao R, Inami T and Katano S 1996 *Phys. Rev. Lett.* **77** 904
[49] Isihara S, Inoue J and Maekawa S 1996 *Preprint*
Koshibae W, Kawamura Y, Isihara S, Okamuto S, Inoue J and Maekawa S 1997 *J. Phys. Soc. Japan* **66** 957
[50] Anisimov V I, Elfimov I S, Korotin M A and Terakura K 1996 *Preprint*
[51] Varma C M 1996 *Phys. Rev.* B **54** 7328
[52] Auerbach A 1994 *Interacting Electrons and Quantum Magnetism* (Berlin: Springer)
[53] Sarker S K 1996 *J. Phys. C: Solid State Phys.* **37** L515
[54] Georges A, Kotliar G, Krauth W and Rozenberg M J 1996 *Rev. Mod. Phys.* **68** 13